

High-accuracy first-principles determination of the structural, vibrational and thermodynamical properties of diamond, graphite, and derivatives

Nicolas Mounet and Nicola Marzari[†]

Department of Materials Science and Engineering,
Massachusetts Institute of Technology, Cambridge, MA, USA
(dated: December 29, 2021)

The structural, dynamical, and thermodynamical properties of diamond, graphite and layered derivatives (graphene, rhombohedral graphite) are computed using a combination of density-functional theory (DFT) total-energy calculations and density-functional perturbation theory (DFPT) lattice dynamics at the GGA-PBE level. Overall, very good agreement is found for the structural properties and phonon dispersions, with the exception of the c/a ratio in graphite and the associated elastic constants and phonon dispersions. Both the C_{33} elastic constant and the Γ -to-A phonon dispersions are brought to close agreement with available data once the experimental c/a is chosen for the calculations. The thermal expansion, the temperature dependence of the elastic moduli and the specific heat have been calculated via the quasi-harmonic approximation. Graphite shows a distinctive in-plane negative thermal-expansion coefficient that reaches them inimum around room temperature, in very good agreement with experiments. Thermal contraction in graphene is found to be three times as large; in both cases, ZA acoustic modes are shown to be responsible for the contraction, in a direct manifestation of the membrane effect predicted by Lifshitz over fifty years ago.

PACS numbers: 63.20.Dj, 65.40.-b, 71.15.Mb, 81.05.Uw

I. INTRODUCTION

The extraordinary variety of carbon allotropes, as well as their present and potential applications in such diverse fields as nanoelectronics¹ or bioengineering², gives them a special place among all the elements. Even excluding fullerenes, nanotubes, and their derivatives, single crystalline diamond, graphite and graphene (i.e. a single graphite layer) still lack a complete characterization of their thermodynamic stability under a broad range of conditions (see e.g. Refs. 3,4,5,6,7 and citations therein). In this respect, vibrational properties play a crucial role in determining the thermodynamic properties of the bulk. Indeed, diamond being a wide band gap material ($E_g = 5.5$ eV), electronic excitations do not account for thermal properties up to high temperatures. Graphite and graphene are semimetals, but the gap vanishes only at the K point where the two massless bands cross (see e.g. Ref. 8); thus, electronic excitations can also be neglected in these materials, and the phonon dispersions provide all the information that is needed to calculate thermodynamical quantities such as the thermal expansion or specific heat.

The aim of this paper is to provide a converged, accurate determination of the structural, dynamical, and thermodynamical properties of diamond, graphite, graphene and rhombohedral graphite from first-principles calculations. Although the phonon spectrum of diamond and its thermal properties have been studied extensively with experiments^{9,10} and calculations¹¹, the phonon spectrum of graphite is still under active investigation^{12,13}, as well as its thermal properties. Graphite in-plane thermal expansion has long been recognized to be negative^{14,15}, and it has even been

suggested^{7,15} that this may be due to the internal stresses related to the large expansion in the c direction (Poisson effect). To resolve some of the open questions, and to provide a coherent picture for these materials, we used extensive ab-initio density-functional theory (DFT) and density-functional perturbation theory (DFPT)^{16,17} calculations. DFT is a very efficient and accurate tool to obtain ground-state and linear-response properties, especially when paired with plane-wave basis sets, which easily allow to reach full convergence with respect to basis size, and ultrasoft pseudo-potentials¹⁸ for optimal performance and transferability. We adopted the PBE-GGA¹⁹ exchange-correlation functional, at variance with most of the early studies on diamond^{11,20,21} and especially graphite^{13,22,23,24,25,26}, which have been performed using the local density approximation (LDA). GGA calculations have appeared mostly for the cases of diamond (GGA-PBE, Ref. 21) and graphene (GGA-PBE, Refs. 12,13), with some data for graphite appearing in Refs. 13,27,28,29 (GGA-PBE). DFPT^{16,17} is then used to compute the phonon frequencies at any arbitrary wavevector, without having to resort to the use of supercells. The vibrational free energy is calculated in the quasi-harmonic approximation (QHA)^{11,30}, to predict finite-temperature lattice properties such as thermal expansion and specific heat.

To the best of our knowledge, this is the first study on the thermal properties of graphite or graphene from first-principles. For the case of diamond and graphene, calculations are fully ab-initio and do not require any experimental input. For the case of graphite and rhombohedral graphite we argue that the use of the experimental c/a greatly improves the agreement with experimental data. This experimental input is required since DFT, in its

current state of development, yields poor predictions for the interlayer interactions, dominated by Van Der Waals dispersion forces not well described by local or semi-local exchange correlation functionals (see Refs. 31 and 32 for details; the agreement between LDA predictions and experimental results for the c/a ratio is fortuitous). It is found that the weak interlayer bonding has a small influence on most of the properties studied and that forcing the experimental c/a corrects almost all the remaining ones. This allowed us to obtain results for all the materials considered that are in very good agreement with the available experimental data.

The article is structured as follows. We give a brief summary of our approach and definitions and introduce DFPT and the QHA in Section II. Our ground-state, zero-temperature results for diamond, graphite, graphene and rhombohedral graphite are presented in Section III: Lattice parameters and elastic constants from the equations of state in subsection IIIA, phonon frequencies and vibrational density of states in subsection IIIB, and first-principles, linear-response interatomic force constants in subsection IIIC. The lattice thermal properties, such as thermal expansion, mode Grüneisen parameters, and specific heat as obtained from the vibrational free energy are presented in section IV. Section V contains our final remarks.

II. THEORETICAL FRAMEWORK

A. Basics of Density-Functional Perturbation Theory

In density-functional theory^{33,34} the ground state electronic density and wavefunctions of a crystal are found by solving self-consistently a set of one-electron equations. In atomic units (used throughout the article), these are

$$\left(-\frac{1}{2} \nabla^2 + V_{\text{SCF}}(\mathbf{r}) \right) \psi_{i\mathbf{i}} = \epsilon_{i\mathbf{i}} \psi_{i\mathbf{i}}; \quad (1a)$$

$$V_{\text{SCF}}(\mathbf{r}) = \sum_{\mathbf{j}} \frac{n(\mathbf{r}^0)}{|\mathbf{r} - \mathbf{r}^0_{\mathbf{j}}|} + \frac{E_{\text{xc}}}{n(\mathbf{r})} + V_{\text{ion}}(\mathbf{r}); \quad (1b)$$

$$n(\mathbf{r}) = \sum_{\mathbf{i}} \sum_{\mathbf{j}} \psi_{i\mathbf{i}}(\mathbf{r}) \psi_{j\mathbf{j}}^*(\mathbf{r}) f(\epsilon_{i\mathbf{i}} - \epsilon_{j\mathbf{j}}); \quad (1c)$$

where $f(\epsilon_{i\mathbf{i}} - \epsilon_{j\mathbf{j}})$ is the occupation function, $\epsilon_{i\mathbf{i}}$ the Fermi energy, E_{xc} the exchange-correlation functional (approximated by GGA-PBE in our case), $n(\mathbf{r})$ the electronic density, and $V_{\text{ion}}(\mathbf{r})$ the ionic core potential (actually a sum over an array of pseudo-potentials).

Once the unperturbed ground state is determined, phonon frequencies can be obtained from the interatomic force constants, i.e. the second derivatives at equilibrium

of the total crystal energy versus displacements of the ions:

$$\begin{aligned} C_{i\mathbf{i}; j\mathbf{j}}(\mathbf{R} - \mathbf{R}^0) &= \frac{\partial^2 E}{\partial u_{i\mathbf{i}}(\mathbf{R}) \partial u_{j\mathbf{j}}(\mathbf{R}^0)}_{\text{equil}} \\ &= C_{i\mathbf{i}; j\mathbf{j}}^{\text{ion}}(\mathbf{R} - \mathbf{R}^0) + C_{i\mathbf{i}; j\mathbf{j}}^{\text{elec}}(\mathbf{R} - \mathbf{R}^0) \end{aligned} \quad (2)$$

Here $\mathbf{R} - \mathbf{R}^0$ is a Bravais lattice vector, $i\mathbf{i}$ ($j\mathbf{j}$) indicates the i^{th} (j^{th}) atom of the unit cell, and $(\)$ represents the cartesian components. $C_{i\mathbf{i}; j\mathbf{j}}^{\text{ion}}$ are the second derivatives¹⁷ of Ewald sums corresponding to the ion-ion repulsion potential, while the electronic contributions $C_{i\mathbf{i}; j\mathbf{j}}^{\text{elec}}$ are the second derivatives of the electron-electron and electron-ion terms in the ground state energy. From the Hellmann-Feynman¹⁷ theorem one obtains:

$$\begin{aligned} C_{i\mathbf{i}; j\mathbf{j}}^{\text{elec}}(\mathbf{R} - \mathbf{R}^0) &= \sum_{\mathbf{r}} \frac{\partial n(\mathbf{r})}{\partial u_{i\mathbf{i}}(\mathbf{R})} \frac{\partial V_{\text{ion}}(\mathbf{r})}{\partial u_{j\mathbf{j}}(\mathbf{R}^0)} \\ &+ n_0(\mathbf{r}) \frac{\partial^2 V_{\text{ion}}(\mathbf{r})}{\partial u_{i\mathbf{i}}(\mathbf{R}) \partial u_{j\mathbf{j}}(\mathbf{R}^0)} d^3 r \end{aligned} \quad (3)$$

(where the dependence of both $n(\mathbf{r})$ and $V_{\text{ion}}(\mathbf{r})$ on the displacements has been omitted for clarity, and $V_{\text{ion}}(\mathbf{r})$ is considered local).

It is seen that the electronic contribution can be obtained from the knowledge of the linear response of the system to a displacement. The key assumption is then the Born-Oppenheimer approximation which views a lattice vibration as a static perturbation on the electrons. This is equivalent to say that the response time of the electrons is much shorter than that of ions, that is, each time ions are slightly displaced by a phonon, electrons instantaneously rearrange themselves in the state of minimum energy of the new ionic configuration. Therefore, static linear response theory can be applied to describe the behavior of electrons upon a vibrational excitation.

For phonon calculations, we consider a periodic perturbation V_{ion} of wave-vector \mathbf{q} , which modifies the self-consistent potential V_{SCF} by an amount δV_{SCF} . The linear response in the charge density $n(\mathbf{r})$ can be found using first-order perturbation theory. If we consider its Fourier transform $n(\mathbf{q} + \mathbf{G})$, and calling $\psi_{o\mathbf{k}}$ the one-particle wavefunction of an electron in the occupied band o at the point \mathbf{k} of the Brillouin zone (and $\epsilon_{o\mathbf{k}}$ the corresponding eigenvalue), one can get a self-consistent set of linear equations similar to Eqs. (1a,1b,1c)³⁵:

$$(\epsilon_{o\mathbf{k}} + \frac{1}{2} \nabla^2 - V_{\text{SCF}}(\mathbf{r})) \psi_{o\mathbf{k}+\mathbf{q}} = \hat{P}_e^{k+\mathbf{q}} V_{\text{SCF}}^{\mathbf{q}} \psi_{o\mathbf{k}} \quad (4a)$$

$$n(\mathbf{q} + \mathbf{G}) = \frac{4}{V} \sum_{\mathbf{k}, j} h_{\mathbf{e}, \mathbf{k}} \hat{P}_{\mathbf{e}}^{i(\mathbf{q} + \mathbf{G})} \hat{P}_{\mathbf{e}}^{k + \mathbf{q}, j} \quad (4b)$$

$$V_{SCF}(\mathbf{r}) = \sum_j \frac{n(\mathbf{r}^0_j)}{r^0_j} \alpha^3 r^0_j + n(\mathbf{r}) \frac{d}{dn} \left(\frac{E_{xc}}{n(\mathbf{r})} \right)_{n_0(\mathbf{r})} + V_{ion}(\mathbf{r}) \quad (4c)$$

$\hat{P}_{\mathbf{e}}^{k + \mathbf{q}}$ refers to the projector on the empty-state manifold at $\mathbf{k} + \mathbf{q}$, V to the total crystal volume, and \mathbf{G} to any reciprocal lattice vector. Note that the linear response contains only Fourier components of wave vector $\mathbf{q} + \mathbf{G}$, so we added a superscript \mathbf{q} to $V_{SCF}^{\mathbf{q}}$. We have implicitly assumed for simplicity that the crystal has a band gap and that pseudo-potentials are local, but the generalization to metals³⁶ and to non-local pseudo-potentials¹⁷ are all well established (see Ref. 16 for a detailed and complete review of DFPT).

Linear-response theory allows us to calculate the response to any periodic perturbation; i.e. it allows direct access to the dynamical matrix related to the interatomic force constants via a Fourier transform:

$$\tilde{D}_{ij}(\mathbf{q}) = \frac{1}{M_i M_j} \sum_{\mathbf{R}} C_{ij}(\mathbf{R}) e^{i\mathbf{q} \cdot \mathbf{R}} \quad (5)$$

(where M_i is the mass of the i^{th} atom).

Phonon frequencies at any \mathbf{q} are the solutions of the eigenvalue problem:

$$\omega^2(\mathbf{q}) u_i(\mathbf{q}) = \sum_j u_j(\mathbf{q}) \tilde{D}_{ij}(\mathbf{q}) \quad (6)$$

In practice, one calculates the dynamical matrix on a relatively coarse grid in the Brillouin zone (say, a $8 \times 8 \times 8$ grid for diamond), and obtains the corresponding interatomic force constants by inverse Fourier transform (in this example it would correspond to a $8 \times 8 \times 8$ supercell in real space). Finally, the dynamical matrix (and phonon frequencies) at any \mathbf{q} point can be obtained by Fourier interpolation of the real-space interatomic force constants.

B. Thermodynamical properties

When no external pressure is applied to a crystal, the equilibrium structure at any temperature T can be found by minimizing the Helmholtz free energy $F(\mathbf{f}_{\mathbf{a}i\mathbf{g}}; T) = U - TS$ with respect to all its geometrical degrees of freedom $\mathbf{f}_{\mathbf{a}i\mathbf{g}}$. If now the crystal is supposed to be perfectly harmonic, F is the sum of the ground state total energy and the vibrational free energy coming from the partition function (in the canonical ensemble) of a collection

of independent harmonic oscillators. In a straightforward manner, it can be shown³⁷ that:

$$\begin{aligned} F(\mathbf{f}_{\mathbf{a}i\mathbf{g}}; T) &= E(\mathbf{f}_{\mathbf{a}i\mathbf{g}}) + F_{\text{vib}}(T) \\ &= E(\mathbf{f}_{\mathbf{a}i\mathbf{g}}) + \sum_{\mathbf{q}, j} \frac{\hbar \omega_{\mathbf{q}, j}}{2} \\ &\quad + k_B T \sum_{\mathbf{q}, j} \ln \left(1 - \exp \left(-\frac{\hbar \omega_{\mathbf{q}, j}}{k_B T} \right) \right) \end{aligned} \quad (7)$$

where $E(\mathbf{f}_{\mathbf{a}i\mathbf{g}})$ is the ground state energy and the sum is run over all the Brillouin zone wave-vectors and the band index j of the phonon dispersion. The second term in the right hand side of Eq.(7) is the zero-point motion.

If anharmonic effects are neglected, the phonon frequencies do not depend on lattice parameters, therefore the free energy dependence on structure is entirely contained in the ground state equation of state $E(\mathbf{f}_{\mathbf{a}i\mathbf{g}})$. Consequently the structure does not depend on temperature in a harmonic crystal.

Thermal expansion is recovered by introducing in Eq.(7) the dependence of the phonon frequencies on the structural parameters $\mathbf{f}_{\mathbf{a}i\mathbf{g}}$; direct minimization of the free energy

$$\begin{aligned} F(\mathbf{f}_{\mathbf{a}i\mathbf{g}}; T) &= E(\mathbf{f}_{\mathbf{a}i\mathbf{g}}) + F_{\text{vib}}(\omega_{\mathbf{q}, j}(\mathbf{f}_{\mathbf{a}i\mathbf{g}}); T) \\ &= E(\mathbf{f}_{\mathbf{a}i\mathbf{g}}) + \sum_{\mathbf{q}, j} \frac{\hbar \omega_{\mathbf{q}, j}(\mathbf{f}_{\mathbf{a}i\mathbf{g}})}{2} \\ &\quad + k_B T \sum_{\mathbf{q}, j} \ln \left(1 - \exp \left(-\frac{\hbar \omega_{\mathbf{q}, j}(\mathbf{f}_{\mathbf{a}i\mathbf{g}})}{k_B T} \right) \right) \end{aligned} \quad (8)$$

provides the equilibrium structure at any temperature T . This approach goes under the name quasi-harmonic approximation (QHA) and has been applied successfully to many bulk systems^{1,38,39}. The linear thermal expansion coefficients of the cell dimensions of a lattice are then

$$\alpha_i = \frac{1}{a_i} \frac{\partial a_i}{\partial T} \quad (9)$$

The Grüneisen formalism⁴⁰ assumes a linear dependence of the phonon frequencies on the three orthogonal cell dimensions $\mathbf{f}_{\mathbf{a}i\mathbf{g}}$; developing the ground state energy up to second order, (thanks to the equation of state at $T = 0\text{K}$), one can get from the condition $\frac{\partial F}{\partial a_i} = 0$ the alternative expression

$$\alpha_i = \sum_{\mathbf{q}, j} c_v(\mathbf{q}, j) \sum_k \frac{S_{ik}}{V_0} \frac{a_{0,k}}{\omega_{\mathbf{q}, j}} \frac{\partial \omega_{\mathbf{q}, j}}{\partial a_k} \quad (10)$$

We follow here the formalism of Ref. 41: $c_v(\mathbf{q}, j)$ is the contribution to the specific heat from the mode (\mathbf{q}, j) ,

S_{ik} is the elastic compliance matrix, and the subscript "0" indicates a quantity taken at the ground state lattice parameter. The Grüneisen parameter of the mode $(q;j)$ is by definition

$$\gamma(q;j) = \frac{a_{0;j}}{a_0} \frac{\partial a_0}{\partial a} \quad (11)$$

For a structure which depends only on one lattice parameter a (e.g. diamond or graphene) one then gets for the linear thermal expansion coefficient

$$\alpha = \frac{1}{d^2 B_0 V_0} \sum_{q;j} c_v(q;j) \frac{a_0}{a} \frac{\partial a_0}{\partial a} \quad (12)$$

where B_0 is defined by $B_0 = V_0 \frac{\partial^2 E}{\partial V^2}$ (V represents the volume of a three-dimensional crystal such as diamond or the surface of a two-dimensional one like graphene), d is the number of dimensions ($d = 3$ for diamond, $d = 2$ for graphene), and V_0 is the volume (or the surface) at equilibrium.

In the case of graphite there are two lattice parameters: a in the basal plane and c perpendicular to the basal plane, so that one gets

$$\alpha_a = \frac{1}{V_0} \sum_{q;j} c_v(q;j) (S_{11} + S_{12}) \frac{a_0}{2a} \frac{\partial a_0}{\partial a} + S_{13} \frac{c_0}{a} \frac{\partial a_0}{\partial c} \quad (13a)$$

$$\alpha_c = \frac{1}{V_0} \sum_{q;j} c_v(q;j) S_{13} \frac{a_0}{a} \frac{\partial a_0}{\partial a} + S_{33} \frac{c_0}{c} \frac{\partial a_0}{\partial c} \quad (13b)$$

The mode Grüneisen parameters provide useful insight to the thermal expansion mechanisms. They are usually positive, since phonon frequencies decrease when the solid expands, although some negative mode Grüneisen parameters for low-frequency acoustic modes can arise and sometimes compete with the positive ones, giving a negative thermal expansion at low temperatures, when only the lowest acoustic modes can be excited.

Finally, the heat capacity of the unit cell at constant volume can be obtained from $C_v = T \frac{\partial^2 F_{vib}}{\partial T^2}$:³⁷

$$C_v = \sum_{q;j} c_v(q;j) = k_B \sum_{q;j} \frac{\hbar^2 \omega_{q;j}^2}{2k_B T} \frac{1}{\sinh^2 \frac{\hbar \omega_{q;j}}{2k_B T}} \quad (14)$$

C. Computational details

All the calculations that follow were performed using the ESPRESSO⁴² package, which is a full ab-initio DFT and DFPT code available under the GNU Public License⁴³. We used a plane-wave basis set, ultrasoft pseudo-potentials¹⁸ from the standard distribution⁴⁴ (generated using a modified RKKJ⁴⁵ approach), and the generalized gradient approximation (GGA) for the exchange-correlation functional in its PBE parameterization¹⁹. We also used the local density approximation (LDA) in order to compare some results between the two functionals. In this case the parameterization used was the one proposed by Perdew and Zunger⁴⁶.

For the semimetallic graphite and graphene cases, we used 0.03 Ryd of cold smearing⁴⁷. We carefully and extensively checked the convergence in the energy differences between different configurations and the phonon frequencies with respect to the wavefunction cutoff, the dual (i.e. the ratio between charge density cutoff and wavefunction cutoff), the k-point sampling of the Brillouin zone, and the interlayer vacuum spacing for graphene. Energy differences were converged within 5 meV/atom or better, and phonon frequencies within 1 cm⁻¹. In the case of graphite and graphene phonon frequencies were converged with respect to the k-point sampling after having set the smearing parameter at 0.03 Ryd. Besides, values of the smearing between 0.02 Ryd and 0.04 Ryd did not change the frequencies by more than 1 cm⁻¹.

In a solid, translational invariance guarantees that three phonon frequencies at Γ will go to zero. In our GGA-PBE-DFPT formalism this condition is exactly satisfied only in the limit of infinite k-point sampling and full convergence with the plane-wave cutoff. For the case of graphene and graphite we found in particular that an exceedingly large cutoff (100 Ryd) and dual (28) would be needed to recover phonon dispersions (especially around Γ and the A branch) with the tolerances mentioned; on the other hand, application of the acoustic sum rule (i.e. forcing the translational symmetry on the interatomic force constants) allows us to recover these highly converged calculations above with a more reasonable cutoff and dual.

Finally, the cutoffs we used were 40 Ryd for the wavefunctions in all the carbon materials presented, with duals of 8 for diamond and 12 for graphite and graphene. We used a 8 × 8 × 8 Monkhorst-Pack k-mesh for diamond, 16 × 16 × 8 for graphite, 16 × 16 × 4 for rhombohedral graphite and 16 × 16 × 1 for graphene. All these meshes were unshifted (i.e. they do include Γ). Dynamical matrices were initially calculated on a 8 × 8 × 8 q-points mesh for diamond, 8 × 8 × 4 for graphite, 8 × 8 × 2 for rhombohedral graphite and 16 × 16 × 1 for graphene.

Finally, integrations over the Brillouin zone for the vibrational free energy or the heat capacity were done using phonon frequencies that were Fourier interpolated on much finer meshes. The phonon frequencies were usually

TABLE I: Equilibrium lattice parameter a_0 and bulk modulus B_0 of diamond at the ground state (GS) and at 300 K (see Section IV), compared to experimental values.

	Present calculation	Experiment (300 K)
Lattice constant a_0	6.743 (GS)	6.740 ^a
(a.u.)	6.769 (300 K)	
Bulk modulus B_0	432 (GS)	442 ^b
(GPa)	422 (300 K)	

^aRef. 49

^bRef. 50

computed at several lattice parameters and the results interpolated to get their dependence on lattice constants.

A final remark is that we were careful to use the same parameters (cutoffs, k-points sampling, smearing, etc.) in the determination of the ground state equation of state and that of the phonon frequencies, since these two terms need to be added in the free energy expression.

III. ZERO-TEMPERATURE RESULTS

A. Structural and elastic properties

We performed ground state total-energy calculations on diamond, graphite, and graphene over a broad range of lattice parameters. The potential energy surface can then be fitted by an appropriate equation of state. The minimum gives the ground state equilibrium lattice parameter(s). The second derivatives at that minimum are related to the bulk modulus or elastic constants.

For the case of diamond we chose the Birch equation of state⁴⁸ (up to the fourth order) to fit the total energy vs. the lattice constant a :

$$E(a) = E_0 + \frac{9}{8}B_0V_0 \left(\frac{a_0}{a} \right)^2 + A \left(\frac{a_0}{a} \right)^3 + B \left(\frac{a_0}{a} \right)^4 + O \left(\frac{a_0}{a} \right)^5 \quad (15)$$

where B_0 is the bulk modulus, V_0 the primitive cell volume ($V_0 = \frac{a^3}{4}$ here) and A and B are fit parameters. The Mumaghan equation of state or even a polynomial would fit equally well the calculations around the minimum of the curve. A best fit of this equation on our data gives us both the equilibrium lattice parameter and the bulk modulus; our results are summarized in Table I. The agreement with the experimental values is very good, even after the zero-point motion and thermal expansion are added to our theoretical predictions (see Section IV).

The ground state equation of state of graphene was fitted by a 4th order polynomial, and the minimum found for $a = 4.654$ a.u., which is very close to the experimental in-plane lattice parameter of graphite. The graphite

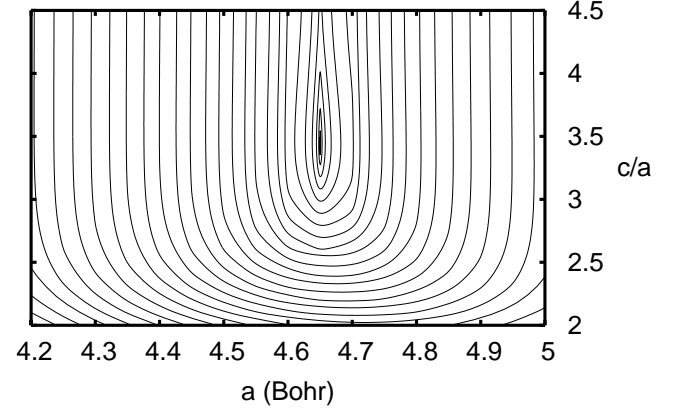


FIG. 1: Contour plot of the ground state energy of graphite as a function of a and c/a (isoenergy contours are not equidistant).

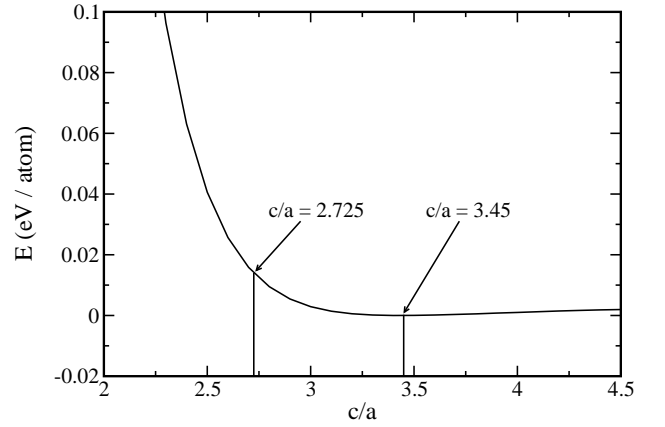


FIG. 2: Ground state energy of graphite as a function of c/a at fixed $a = 4.65$ a.u.. The theoretical (PBE) and the experimental c/a are shown. The zero of energy has been set to the PBE minimum.

equation of state was fitted by a two-dimensional 4th order polynomial of variables a and c . To illustrate the very small dependence of the ground state energy with the c/a ratio, we have plotted the results of our calculations over a broad range of lattice constants in Figs. 1 and 2.

A few elastic constants can be obtained from the second derivatives of this energy²²:

$$\begin{aligned} \text{Stiffness coefficients} \quad C_{11} + C_{12} &= \frac{1}{3c_0} \frac{\partial^2 E}{\partial a^2} \\ C_{33} &= \frac{2c_0}{3a_0^2} \frac{\partial^2 E}{\partial c^2} \\ C_{13} &= \frac{1}{3a_0} \frac{\partial^2 E}{\partial a \partial c} \end{aligned} \quad (16a)$$

$$\text{Tetragonal shear modulus } C^t = \frac{1}{6} [(C_{11} + C_{12}) + 2C_{33} - 4C_{13}] \quad (16b)$$

$$\text{Bulk modulus } B_0 = \frac{C_{33}(C_{11} + C_{12}) + 2C_{13}^2}{6C^t} \quad (16c)$$

We summarize all our LDA and GGA results in Table II: For LDA, both the lattice parameter a_0 and the c_0/a_0 ratio are very close to experimental data. Elastic constants were calculated fully from first-principles, in the sense that the second derivatives of the energy were taken at the theoretical LDA a_0 and c_0 , and that only these theoretical values were used in Eqs. (16a). Elastic constants are found in good agreement with experiments, except for the case of C_{13} which comes out as negative (meaning that the Poisson's coefficient would be negative).

Fully theoretical GGA results (second column of Table II) compare poorly to experimental data except for the a_0 lattice constant, in very good agreement with experiments. Using the experimental value for c_0 in Eqs. (16) improves only the value of $C_{11} + C_{12}$ (third column of Table II). Most of the remaining disagreement is related to the poor value obtained for c/a ; if the second derivatives in Eqs. (16a) are taken at the experimental value for c/a all elastic constants are accurately recovered except for C_{13} (fourth column of Table II).

In both LDA and GGA, errors arise from the fact that Van Der Waals interactions between graphitic layers are poorly described. These issues can still be addressed within the framework of DFT (as shown by Langreth and collaborators, Ref. 31) at the cost of having a non-local exchange-correlation potential.

Zero-point motion and finite-temperature effects will be discussed in detail in Section IV.

B. Phonon dispersion curves

We have calculated the phonon dispersion relations for diamond, graphite, rhombohedral graphite and graphene. For diamond and graphene, we used the theoretical lattice parameter. For graphite, we either used the theoretical c/a or the experimental one ($c/a = 2.725$). We will comment extensively in the following on the role of c/a on our calculated properties.

Finally we also calculated the phonon dispersions for rhombohedral graphite, which differs from graphite only in the stacking of the parallel layers: in graphite the stacking is ABABAB while it is ABCABC in rhombohedral graphite, and the latter unit cell contains six atoms instead of four. We therefore used the same in-plane lattice parameter and same interlayer distance as in graphite (that is, a $\frac{c}{a}$ ratio multiplied by $\frac{3}{2}$). Results are presented in Figs. 3, 4, 5, 6 and 7, together with the experimental

data.

In Table III and IV we summarize our results at high-symmetry points and compare them with experimental data. In diamond, GGA produces softer modes than LDA¹¹ on the whole (as expected), particularly at (optical mode) and in the optical -X branches. For these, the agreement is somehow better in LDA; on the other hand the whole -L dispersion is overestimated by LDA.

The results on graphite require some comments. In Table IV and Figs. 4, 5, 6 and 7, modes are classified as follows: L stands for longitudinal polarization, T for in-plane transversal polarization and Z for out-of-plane transversal polarization. For graphite, a prime (as in LO') indicates an optical mode where the two atoms in each layer of the unit cell oscillate together and in phase opposition to the two atoms of the other layer. A non-primed optical mode is instead a mode where atoms inside the same layer are "optical" with respect to each other. Of course "primed" optical modes do not exist for graphene, since there is only one layer (two atoms) per unit cell.

We observe that stacking has a negligible effect on all the frequencies above 400 cm⁻¹, since both rhombohedral graphite and hexagonal graphite show nearly the same dispersions except for the -A branch and the in-plane dispersions near . The in-plane part of the dispersions is also very similar to that of graphene, except of course for the low optical branches (below 400 cm⁻¹) that appear in graphite and are not present in graphene.

For graphite as well as diamond GGA tends to make the high optical modes weaker while LDA makes them stronger than experimental values. The opposite happens for the low optical modes, and for the -A branch of graphite; the acoustic modes show marginal differences and are in very good agreement with experiments. Overall, the agreement of both LDA and GGA calculations with experiments is very good and comparable to that between different measurements.

Some characteristic features of both diamond and graphite are well reproduced by our ab-initio results, such as the LO branch overbending and the associated shift of the highest frequencies away from . Also, in the case of graphite, rhombohedral graphite and graphene, the quadratic dispersion of the in-plane ZA branch in the vicinity of is observed; this is a characteristic feature of the phonon dispersions of layered crystals^{60,61}, observed experimentally e.g. with neutron scattering⁵⁸. Nevertheless, some discrepancies are found in graphite. The most obvious one is along the -MTA branch, where EELS⁵⁵ data show much higher frequencies than calculations. Additionally several EELS experiments^{56,57} report a gap between the ZA and ZO branches at K while these cross each other in all the calculations. In these cases the disagreement could come either from a failure of DFT within the approximations used or from imperfections in the crystals used in the experiments.

There are also discrepancies between experimental data, in particular in graphite for the LA branch around

TABLE II: Structural and elastic properties of graphite according to LDA, GGA, and experiments

	LDA fully theoretical	GGA fully theoretical	GGA using exp. c_0 in Eqs. (16a)	GGA with 2 nd derivatives taken at exp. $c_0 = a_0$	Experiment (300 K)
Lattice constant a_0 (a.u.)	4.61	4.65	4.65	4.65 (fixed)	4.65 ± 0.003 ^a
$\frac{c_0}{a_0}$ ratio	2.74	3.45	3.45	2.725 (fixed)	2.725 ± 0.001 ^a
$C_{11} + C_{12}$ (GPa)	1283	976	1235	1230	1240 ± 40 ^b
C_{33} (GPa)	29	2.4	1.9	45	36.5 ± 1 ^b
C_{13} (GPa)	-2.8	-0.46	-0.46	-4.6	15 ± 5 ^b
B_0 (GPa)	27.8	2.4	1.9	41.2	35.8 ^c
C^t (GPa)	225	164	207	223	208.8 ^c

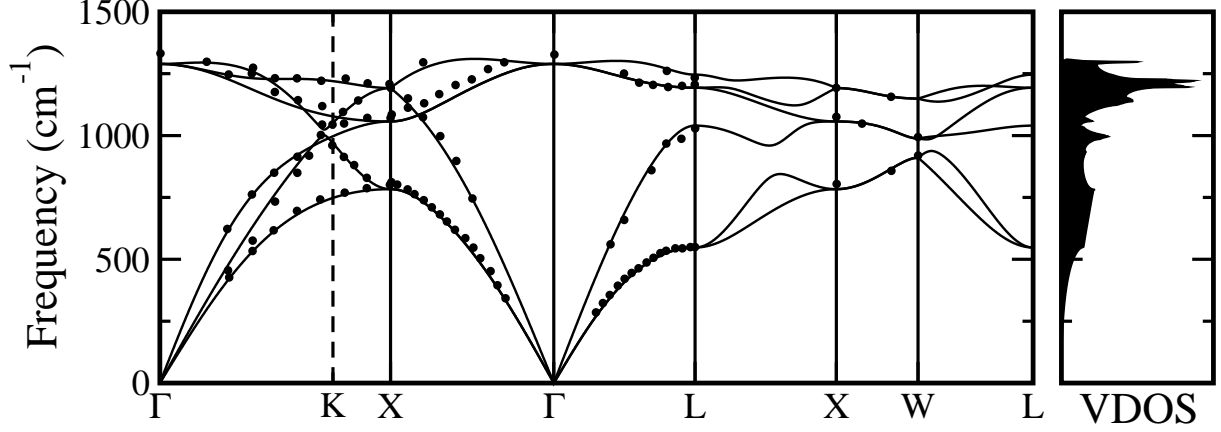
^aRefs. 51,52,53, as reported by Ref. 22.^bRef. 6^cRef. 54, as reported by Ref. 22

FIG. 3: GGA ab-initio phonon dispersions (solid lines) and vibrational density of states (VDOS) for diamond. Experimental neutron scattering data from Ref. 9 are shown for comparison (circles).

TABLE III: Phonon frequencies of diamond at the high-symmetry points Γ , X and L, in cm^{-1} .

	Γ	X_{TA}	X_{TO}	X_{LO}	L_{TA}	L_{LA}	L_{TO}	L_{LO}
LDA ^a	1324	800	1094	1228	561	1080	1231	1275
GGA ^b	1289	783	1057	1192	548	1040	1193	1246
Exp. ^c	1332	807	1072	1184	550	1029	1206	1234

^aRef. 11^bPresent calculation^cRef. 9

K : EELS data from Ref. 56 agree with our ab-initio results while those from Ref. 57 deviate from them.

Finally, we should stress again the dependence of the graphite phonon frequencies on the in-plane lattice parameter and c/a ratio. The results we have analyzed so far were obtained using the theoretical in-plane lattice parameter a and the experimental c/a ratio for both GGA and LDA. Since the LDA theoretical c/a is very close to the experimental one (2.74 vs. 2.725) and the interlayer bonding is very weak, these differences do not matter. However this is not the case for GGA, as the theoretical c/a ratio is very different from the experimental one (3.45 vs. 2.725). Fig. 7 and the second column of

Table IV show results of GGA calculations performed at the theoretical c/a . Low frequencies (below 150 cm^{-1}) between Γ and A are strongly underestimated, as are the ZO' modes between Γ and M, while the remaining branches are barely affected.

The high-frequency optical modes are instead strongly dependent on the in-plane lattice constant. The difference between the values of a in LDA and GGA explains much of the discrepancy between the LDA optical modes and the GGA ones. Indeed, a LDA calculation performed at $a = 4.65 \text{ a.u.}$ and $c/a = 2.725$ (not shown here) brings the phonon frequencies of these modes very close to the GGA ones obtained with the same parameters, while lower-energy modes (below 1000 cm^{-1}) are hardly affected.

Our final choice to use the theoretical in-plane lattice parameter and the experimental c/a seems to strike a balance between the need of theoretical consistency and that of accuracy. Therefore, the remaining of this section is based on calculations performed using the parameters discussed above ($a = 4.61$ for LDA, $a = 4.65$ for GGA and $c/a = 2.725$ in each case).

Elastic constants can be extracted from the data on sound velocities. Indeed, the latter are the slopes of the dispersion curves in the vicinity of Γ and can be ex-

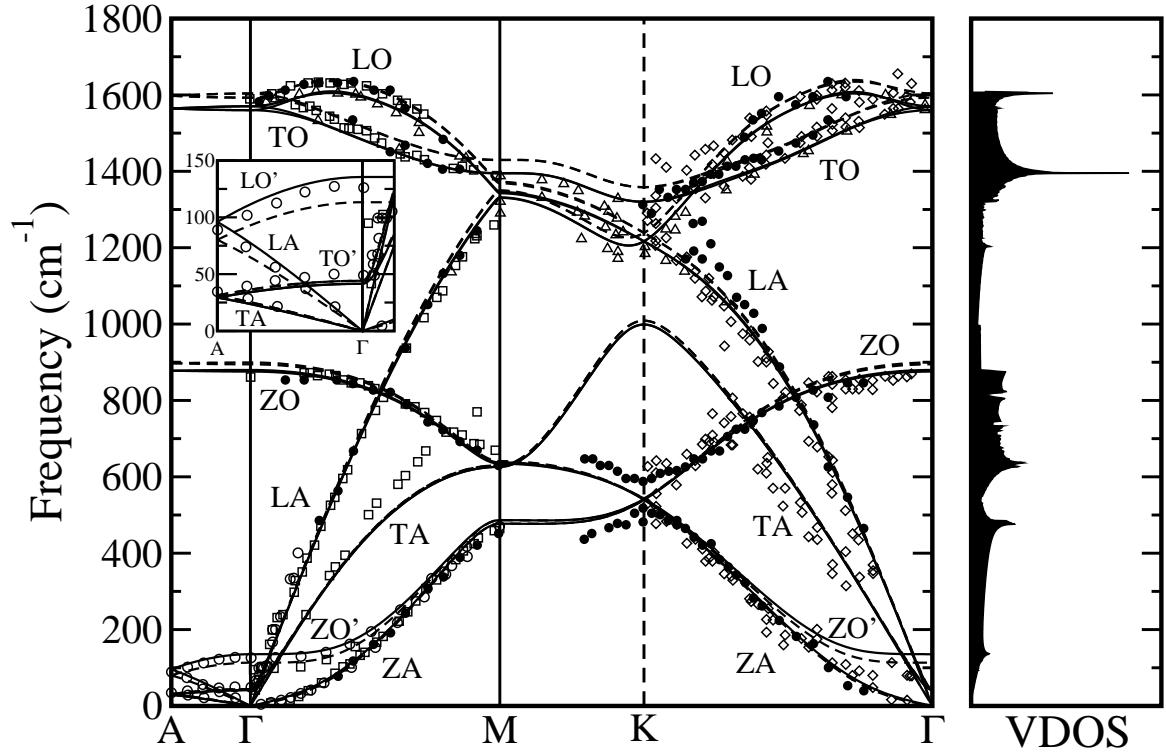


FIG. 4: GGA (solid lines) and LDA (dashed line) ab-initio phonon dispersions for graphite, together with the GGA vibrational density of states (VDOS). The inset shows an enlargement of the low-frequency Γ -A region. The experimental data are EELS (Electron Energy Loss Spectroscopy) from Refs. 55, 56, 57 (respectively squares, diamonds, and filled circles), neutron scattering from Ref. 58 (open circles), and x-ray scattering from Ref. 12 (triangles). Data for Refs. 55 and 57 were taken from Ref. 13.

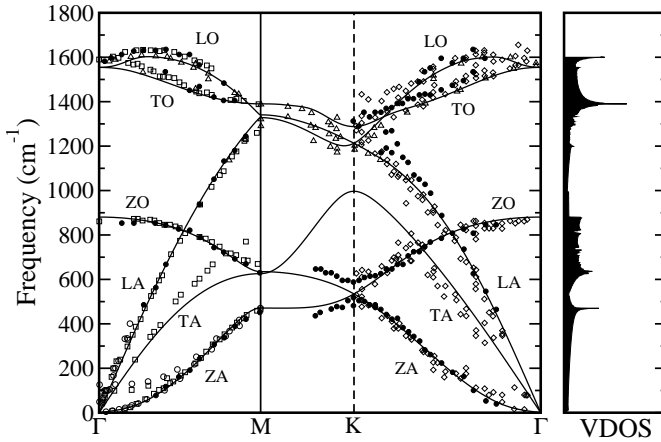


FIG. 5: GGA ab-initio phonon dispersions for graphene (solid lines). Experimental data for graphite are also shown, as in Fig. 4.

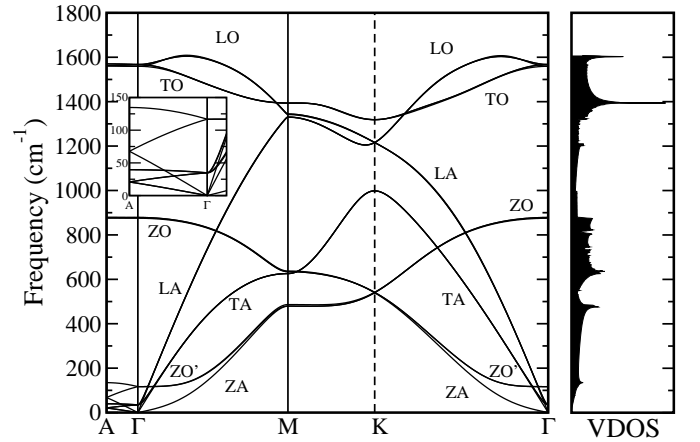


FIG. 6: GGA ab-initio phonon dispersions for rhombohedral graphite. The inset shows an enlargement of the low-frequency Γ -A region.

pressed as the square root of linear combinations of elastic constants (depending on the branch considered) over the density (see Ref. 62 for details). We note in passing that we computed the density consistently with the geometry used in the calculations (see Table IV for details, first column for LDA and third one for GGA), and not the experimental density. Our results are shown in

Table V.

The overall agreement with experiment is good to very good. LDA leads to larger elastic constants, as expected from the general tendency to "overbind", but still agrees well with experiment. For diamond, the agreement is particularly good. As for C_{13} in graphite, it is quite difficult to obtain it from the dispersion curves since it

TABLE IV : Phonon frequencies of graphite and derivatives at the high-symmetry points Γ , M and K , in cm^{-1} . The lattice constants used in the calculations are also shown.

Functional	Graphite			Rhomb. graphite	Graphene	Graphite
	LDA	GGA	GGA	GGA	GGA	Experiment
In-plane lattice ct. a_0	4.61 a.u.	4.65 a.u.	4.65 a.u.	4.65 a.u.	4.65 a.u.	4.65 a.u.
Interlayer distance a_c	1.36	1.725	1.36	1.36	15	1.36
$A_{TA=TO}$	31	6	29			35 ^a
$A_{LA=LO}$	80	20	96			89 ^a
A_{LO}	897	880	878			
A_{TO}	1598	1561	1564			
$L_{O'}$	44	8	41	35		49 ^a
$Z_{O'}$	113	28	135	117		95 ^b , 126 ^a
Z_O	899	881	879	879	881	861 ^b
$L_{O=TO}$	1593	1561	1559	1559	1554	1590 ^b , 1575 ^f
	1604	1561	1567			
M_{ZA}	478	471	477	479	471	471 ^a , 465 ^b , 451 ^d
M_{TA}	630	626	626	626	626	630 ^d
M_{ZO}	637	634	634	635	635	670 ^b
M_{LA}	1349	1331	1330	1330	1328	1290 ^c
M_{LO}	1368	1346	1342	1344	1340	1321 ^c
M_{TO}	1430	1397	1394	1394	1390	1388 ^c , 1389 ^b
K_{ZA}	540	534	540	535	535	482 ^d , 517 ^d , 530 ^e
K_{ZO}	544	534	542	539	535	588 ^d , 627 ^e
K_{TA}	1009	999	998	998	997	
$K_{LA=LO}$	1239	1218	1216	1216	1213	1184 ^c , 1202 ^c
K_{TO}	1359	1308	1319 ^g	1319	1288 ^g	1313 ^d , 1291 ^e

^aRef. 58

^bRef. 55

^cRef. 12

^dRef. 57

^eRef. 56

^fRef. 59

^gNote that a direct calculation of this mode with DFPT (instead of the Fourier interpolation result given here) leads to a significantly lower value in the case of graphite | 1297 cm^{-1} instead of 1319 cm^{-1} . This explains much of the discrepancy between the graphite and graphene result, since in the latter we used a denser q-points mesh. This effect is due to the Kohn anomaly occurring at K²⁹.

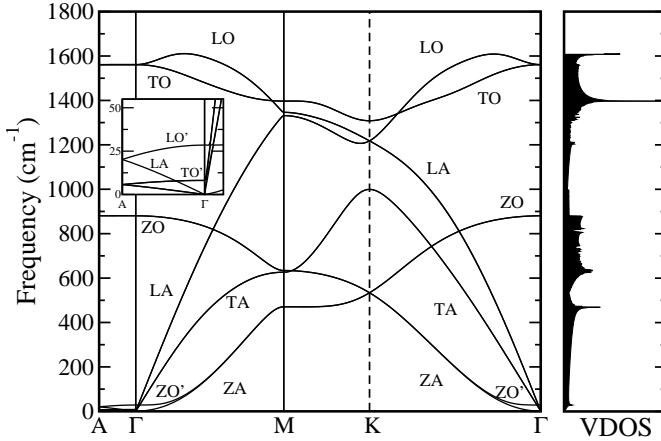


FIG. 7: GGA ab-initio phonon dispersions for graphite at the theoretical $c=a$. The inset shows an enlargement of the low-frequency Γ -A region.

enters the sound velocities only in a linear combination involving other elastic constants, for which the error is almost comparable to the magnitude of C_{13} itself.

An accurate description of the phonon dispersions allows us to predict the low-energy structural excitations

TABLE V : Elastic constants of diamond and graphite as calculated from the phonon dispersions, in GPa.

Functional	D i a m o n d			G r a p h i t e			
	G G A	E x p .		L D A	G G A	E x p .	
C ₁₁	1060	1076.4	0.2 ^b	1118	1079	1060	20 ^a
C ₁₂	125	125.2	2.3 ^b	235	217	180	20 ^a
C ₄₄	562	577.4	1.4 ^b	4.5	3.9	4.5	0.5 ^a
C ₃₃	—	—		29.5	42.2	36.5	1 ^a

^aRef. 6

^bRef. 50

and thus several thermodynamical quantities. Before exploring this in Section IV, we want to discuss the nature and decay of the interatomic force constants in carbon based materials.

C. Interatomic force constants

As explained in Section IIA, the interatomic force constants $C_{ij}(\mathbf{R} - \mathbf{R}^0)$ are obtained in our calculations from the Fourier transform of the dynamical matrix $D'_{ij}(\mathbf{q})$ calculated on a regular mesh inside the Brillouin zone

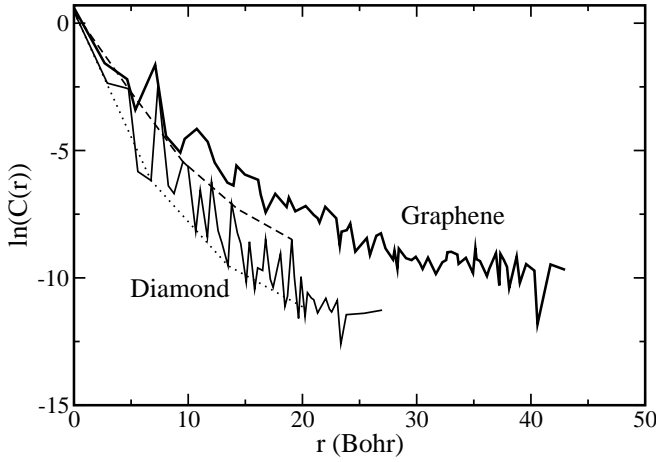


FIG. 8: Decay of the norm of the interatomic force constants as a function of distance for diamond (thin solid line) and graphene (thick solid line), in a semi-logarithmic scale. The dotted and dashed lines show the decay for diamond along the (100) and (110) directions.

(8 8 8 for diamond, 8 8 4 for graphite and 16 16 1 for graphene). This procedure is exactly equivalent (but much more efficient) than calculating the interatomic force constants with frozen phonons (up to 47 neighbors in diamond and 74 in graphene). At a given R , $C_{ij,j}(R)$ is actually a 2^{nd} order tensor, and the decay of its norm (defined as the square root of the sum of the squares of all the matrix elements) with distance is a good measure to know the effect of distant neighbors. In Fig. 8 we have plotted the natural logarithm of such a norm with respect to the distance from a given atom, for diamond and graphene. The norm has been averaged on all the neighbors located at the same distance before taking the logarithm.

The force-constants decay in graphene is slower than in diamond, and it depends much less on direction. In diamond decay along (110) is much slower than in other directions due to long-range elastic effects along the covalent bonds. This long-range decay is also responsible for the flattening of the phonon dispersions in zincblende and diamond semiconductors along the K - X line (see Fig. 3 and Ref. 17, for instance).

In Fig. 9 we show the decay plot for graphite and graphene, averaged over all directions. The graphite interatomic force constants include values corresponding to graphene (in-plane nearest neighbors) and smaller values corresponding to the weak interlayer interactions.

It is interesting to assess the effects of the truncation of these interatomic force constants on the phonon dispersion curves. This can be done by replacing the force constants corresponding to distant neighbors by zero. In this way the relevance of short-range and long-range contributions can be examined. The former are relevant for short-range force-constant models such as the VFF (Valence Force Field)⁸ or the 4NNFC (4th Nearest-Neighbor Force Constant)⁶³ used e.g. in graphene. Note however

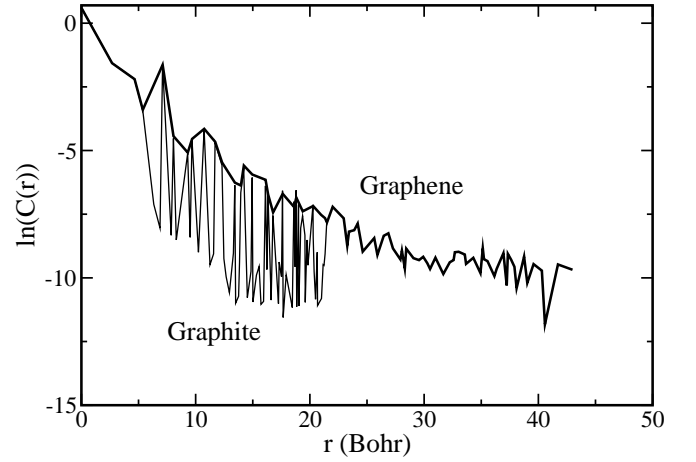


FIG. 9: Decay of the norm of the interatomic force constants as a function of distance for graphite (thin solid line) and graphene (thick solid line).

that a simple truncation is not comparable to the VFF or 4NNFC models, where effective interatomic force constants would be renormalized.

Figs. 10 and 11 show the change in frequency for selected modes in diamond and graphene as a function of the truncation range. The modes we chose are those most strongly affected by the number of neighbors included.

For diamond, our whole supercell contains up to 47 neighbors, and the graph shows only the region up to 20 neighbors included, since the selected modes do not vary by more than 1 cm^{-1} after that. With 5 neighbors, phonon frequencies are already near their converged value, being off by at worst 4% ; very good accuracy (5 cm^{-1}) is obtained with 13 neighbors.

For graphene, our 16 16 1 supercell contains up to 74 neighbors, but after the 30th no relevant changes occur. At least 4 neighbors are needed for the optical modes to be converged within 5-8%. Some acoustic modes require more neighbors, as also pointed out in Ref. 24. As can be seen in Fig. 11, the frequency of some ZA modes in the $-M$ branch (at about one fourth of the branch) oscillates strongly with the number of neighbors included, and can even become imaginary when less than 13 are used, resulting into an instability of the crystal. This behavior does not appear in diamond. Also, the K_{TO} mode keeps varying in going down from 20 to 30 neighbors, though this effect remains small ($8-9 \text{ cm}^{-1}$). This drift could signal the presence of a Kohn anomaly⁶⁴. Indeed, at the K point of the Brillouin zone the electronic band gap vanishes in graphene, so that a singularity arises in the highest optical phonon mode. Therefore a finer q -point mesh is needed around this point, and longer-ranged interatomic force constants. This effect is discussed in detail in Ref. 29.

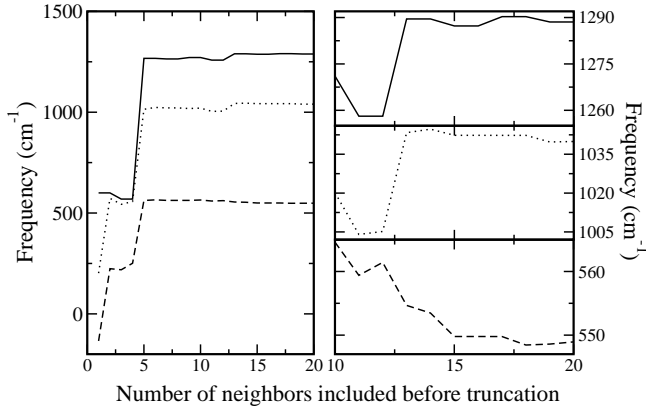


FIG. 10: Phonon frequencies of diamond as a function of the number of neighbors included in the interatomic force constants: \circ (solid line), \times T_O (dotted line), and L_{TA} (dashed line).

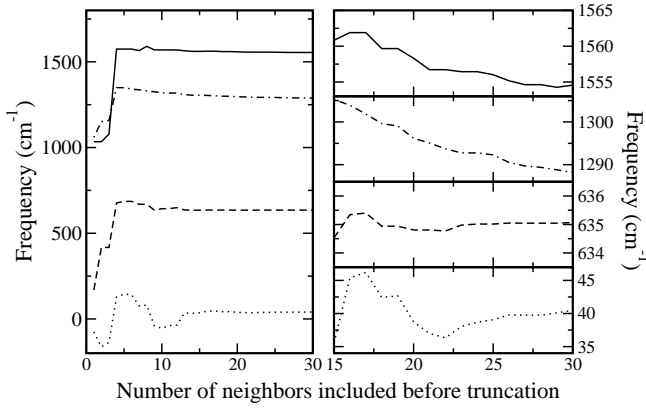


FIG. 11: Phonon frequencies of graphene as a function of the number of neighbors included in the interatomic force constants: $L_{O=TO}$ (solid line), K_{TO} (dot-dashed), M_{ZO} (dashed), and for the dotted line a phonon mode in the ZA branch one-fourth along the Γ to M line.

IV. THERMODYNAMICAL PROPERTIES

We present in this final section our results on the thermodynamical properties of diamond, graphite and graphene using the quasi-harmonic approximation and phonon dispersions at the GGA level. As outlined in Section II B we first perform a direct minimization over the lattice parameter(s) a_i of the vibrational free energy $F(a_i; T)$ (Eq. 8). This gives us, for any temperature T , the equilibrium lattice parameter(s), shown in Figs. 12, 13 and 14. For diamond and graphene, we used in Eq. 8 the equations of state obtained from the ground state calculations presented in Section III A. For graphite this choice would not be useful or accurate, since the theoretical c/a is much larger than the experimental one. So we forced the equation of state to be a minimum for $a = 4.65$ a.u. and $\frac{c}{a} = 2.725$ (fixing only c/a and relaxing a would give $a = 4.66$ a.u., with negligible effects on the thermal

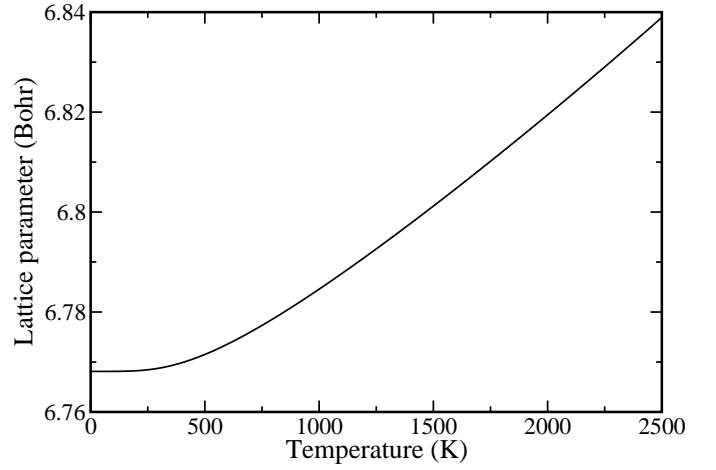


FIG. 12: Lattice parameter of diamond as a function of temperature

expansion). In particular, our "corrected" equation of state is obtained by fitting with a fourth order polynomial the true equation of state around the experimental a and c/a , and then dropping from this polynomial the linear order terms. Since the second derivatives of the polynomial are unchanged, this is to say we keep the elastic constants unchanged. The only input from experiments remains the c/a ratio. We have also checked the effect of imposing to C_{13} its experimental value (C_{13} is the elastic constant that is less accurately predicted), but the changes were small.

The dependence of the phonon frequencies on the lattice parameters was determined by calculating the whole phonon dispersions at several values and interpolating these in between. For diamond and graphene we used four different values of a (from 6.76 to 6.85 a.u. for diamond, and from 4.654 to 4.668 a.u. for graphene) and interpolated them with a cubic polynomial. For graphite, since the minimization space is two dimensional, we restricted ourselves to a linear interpolation and calculated the phonon dispersions at three different combinations of the lattice constants: $(a; c/a) = (4.659, 2.725)$, $(4.659, 2.9)$ and $(4.667, 2.725)$.

Before considering thermal expansion, we examine the zero-point motion. Indeed, lattice parameters at 0 K are different from their ground state values. The effects of the thermal expansion (or contraction) up to about 1000 K are small compared to the zero-point expansion of the lattice parameters. In diamond, a expands from 6.743 a.u. (ground state value) to 6.768 a.u., a difference of 0.4%. For graphene, a is 4.654 a.u. at the ground state and 4.668 a.u. with zero-point motion corrections (+ 0.3%); for graphite a increases from 4.65 to 4.664 a.u. (+ 0.3%) and c from 12.671 to 12.711 (+ 0.3%). The increase is similar in each case, and comparable to the discrepancy between experiments and GGA or LDA ground states.

The coefficients of linear thermal expansion at any T

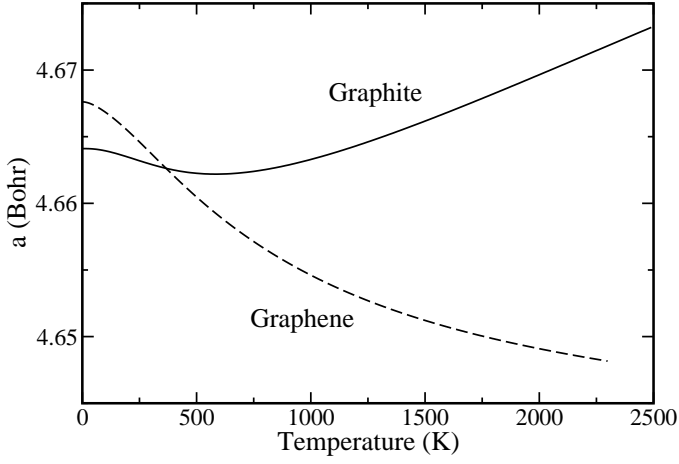


FIG. 13: In-plane lattice parameter of graphite (solid line) and graphene (dashed line) as a function of temperature

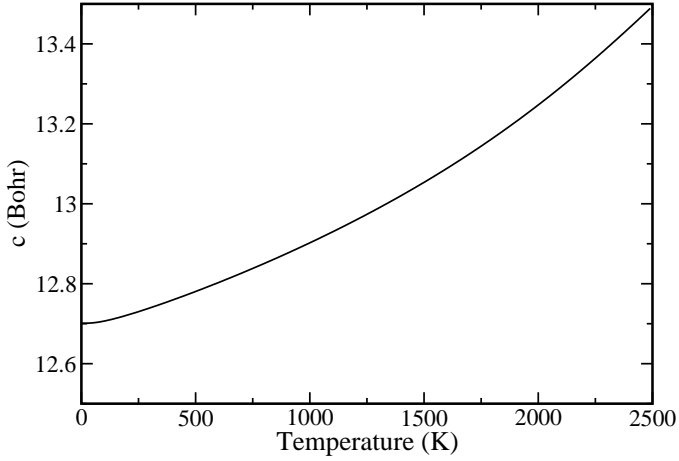


FIG. 14: Out-of-plane lattice parameter of graphite as a function of temperature

are obtained by numerical differentiation of the previous data. Results are shown in Figs. 15, 16 and 17.

For the case of diamond, we have also plotted the linear thermal expansion coefficient calculated using the Grüneisen formalism (Eq. 12) instead of directly minimizing the free energy. While at low temperature the two curves agree, a discrepancy becomes notable above 1000 K, and direct minimization should be performed. This difference between Grüneisen theory and direct minimization seems to explain much of the discrepancy between the calculations of Ref. 11 and our results. Finally a Monte-Carlo path integral study by Herrero and Ramirez⁶⁵, which does not use the QHA, gives very similar results.

For graphite, the in-plane coefficient of linear thermal expansion slightly overestimates the experimental values, but overall the agreement remains excellent, even at high temperatures. Out-of-plane, the agreement holds well up to 150 K, after which the coefficient of linear thermal

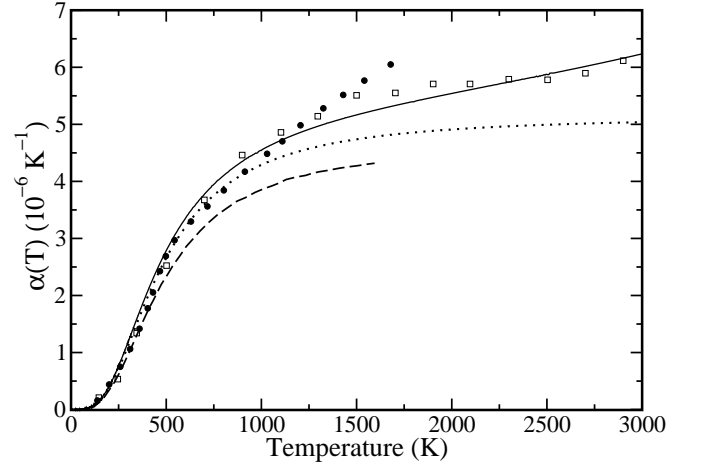


FIG. 15: Coefficient of linear thermal expansion for diamond as a function of temperature. We compare our QHA-GGA ab-initio calculations (solid line) to experiments (Ref. 10, filled circles), a path integral Monte-Carlo study using a Terser empirical potential (Ref. 65, open squares) and the QHA-LDA study by Pavone et al.¹¹ (dashed line). The QHA-GGA thermal expansion calculated using the Grüneisen equation (Eq. 12) is also shown (dotted line).

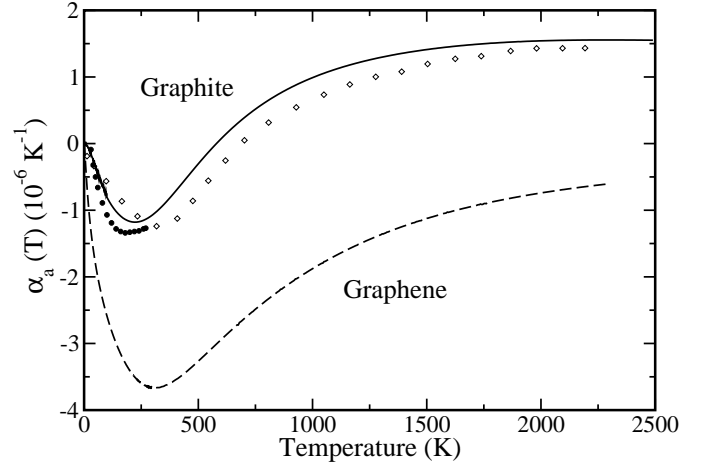


FIG. 16: In-plane coefficient of linear thermal expansion as a function of temperature for graphite (solid line) and graphene (dashed line) from our QHA-GGA ab-initio study. The experimental results for graphite are from Ref. 14 (filled circles) and Ref. 7 (open diamonds).

expansion is underestimated by about 30% at 1000 K.

In-plane, the coefficient of linear thermal expansion is confirmed to be negative from 0 to about 600 K. This feature, absent in diamond, is much more apparent in graphene, where the coefficient of linear thermal expansion keeps being negative up to 2300 K. This thermal contraction will likely appear also in single-walled nanotubes (one graphene sheet rolled on itself)⁶⁶. Some molecular dynamics calculations^{41,67} have already pointed out this characteristic of SWNT.

To further analyze thermal contraction, we plotted

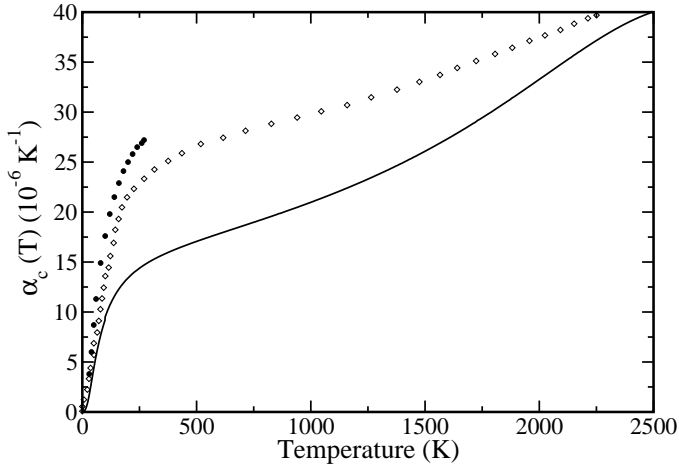


FIG. 17: Out-of-plane coefficient of linear thermal expansion as a function of temperature for graphite from our QHA-GGA ab-initio study (solid line). The experimental results are from Ref. 14 (filled circles), and Ref. 7 (open diamonds).

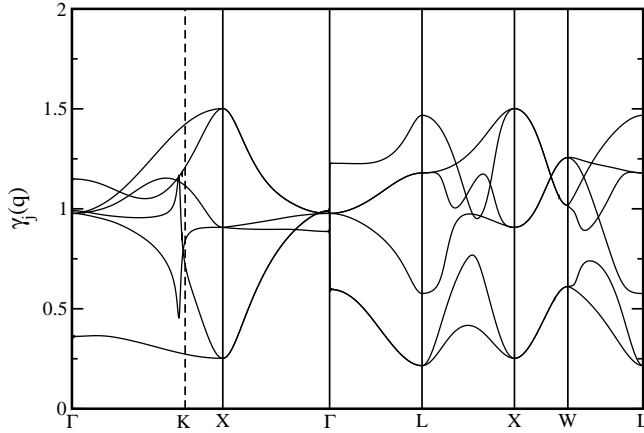


FIG. 18: Ab-initio mode Grüneisen parameters for diamond.

in Figs. 18, 19, 20 and 21 the mode Grüneisen parameters (see Section II B) of diamond, graphene and graphite. These have been obtained from an interpolation of the phonon frequencies by a quadratic (or linear, for graphite) polynomial of the lattice constants, and computed at the ground state lattice parameter.

The diamond Grüneisen parameters have been already calculated with LDA (see Refs. 11,20); our GGA results agree very well with these. In particular, all the Grüneisen parameters are shown to be positive (at odds with other group IV semiconductors such as Si or Ge). The situation is very different in graphite and graphene, where some bands display large and negative Grüneisen parameters (we have used the definition

$$\gamma_j(q) = \frac{a}{2\omega_j(q)} \frac{d\omega_j(q)}{da}.$$

While not visible in the figure, the Grüneisen parameter for the lowest acoustic branch of graphite becomes as low as -40, and as low as -80 for graphene. Therefore, at low temperatures (where most optical modes with posi-

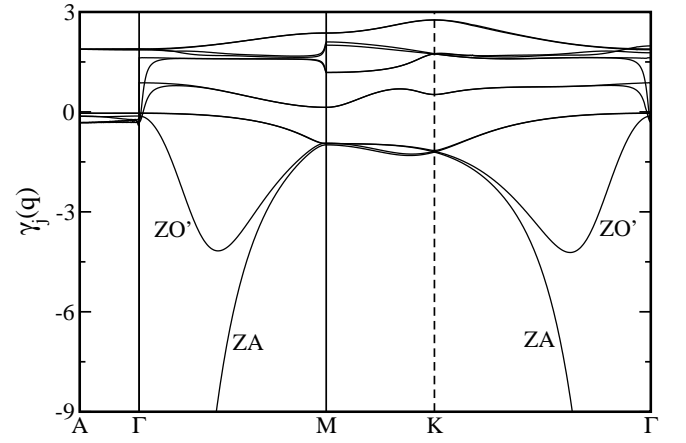


FIG. 19: Ab-initio in-plane mode Grüneisen parameters for graphite.

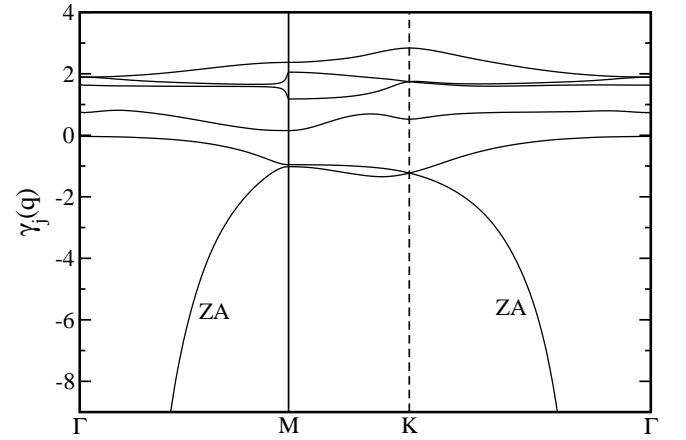


FIG. 20: Ab-initio mode Grüneisen parameters for graphene.

tive Grüneisen parameters are still not excited) the contribution from the negative Grüneisen parameters will be predominant and thermal expansion (from Eq. 12) negative.

The negative Grüneisen parameters correspond to the lowest transversal acoustic (ZA) modes, and in the case of graphite to the (ZO') modes, which can be described as "acoustic" inside the layer and optical out-of-plane (see Section III B). Indeed, the phonon frequencies for such modes increase when the in-plane lattice parameter is increased, contrary to the usual behavior, because the layer is more "stretched" when a is increased, and atoms in that layer will be less free to move in the z direction (just like a rope that is stretched will have vibrations of smaller amplitude, and higher frequency). In graphite these parameters are less negative because of the interaction between layers: atoms are less free to move in the z -direction than in the case of graphene.

This effect, known as the "membrane effect", was predicted by Lifshitz⁶¹ in 1952, when he pointed out the role of these ZA modes (also called "bending modes") in layered materials. In particular, several recent stud-

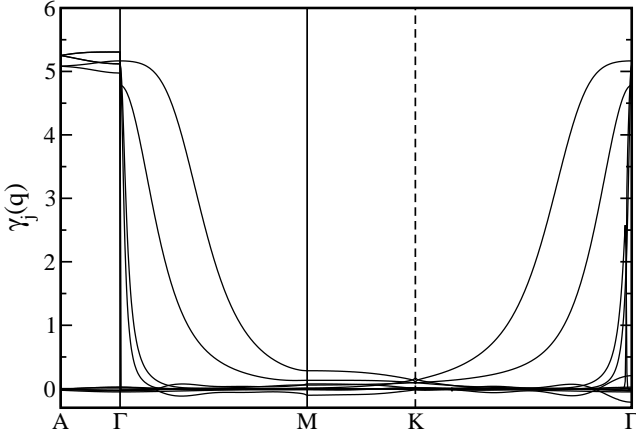


FIG. 21: Ab-initio out-of-plane mode Grüneisen parameters for graphite.

ies have highlighted the relevance of these modes to the thermal properties of layered crystals such as graphite, boron nitride and gallium sulfide^{68,69,70}.

The knowledge of the equilibrium lattice constant(s) at any temperature allows us also to calculate the dependence of elastic constants on temperature. To do so we calculated the second derivatives of the free energy (Eq. 8) vs. lattice constant(s) at the finite-temperature equilibrium lattice parameter(s). We checked that this was equivalent to a best fit of the free energy at T around the equilibrium lattice parameter(s).

Results are shown in Figs. 22 and 23 (diamond and graphite respectively). Again, the zero-point motion has a significant impact on the elastic constants; the agreement with experimental data for the temperature dependence of the ratio of the bulk modulus of diamond to its 298 K value is excellent (upper panel of Fig. 22).

We note that the temperature dependence of the bulk modulus of diamond has already been obtained by Karch et al.⁷¹ using LDA calculations.

As a thermodynamic quantities, we present results on the heat capacities for all the systems considered, at constant volume (C_V) and constant pressure (C_P). C_V has been computed using Eq. 14, in which we used at each temperature T the interpolated phonon frequencies calculated at the lattice constant(s) that minimize the respective free energy. To calculate C_P , we added to C_V the additional term $C_P - C_V = TV_0B_0\alpha_V^2$ where V_0 is the unit cell volume, α_V the volumetric thermal expansion and B_0 the bulk modulus. All these quantities were taken from our ab-initio results and evaluated at each of the temperatures considered. The difference between C_P and C_V is very small, at most about 2% of the value of C_V for graphite and 5% for diamond. Note that C_P and C_V shown on the figures are normalized by dividing by the unit cell mass.

The heat capacity of diamond, graphite and graphene are almost identical except at very low temperatures. Agreement with experimental data is very good.

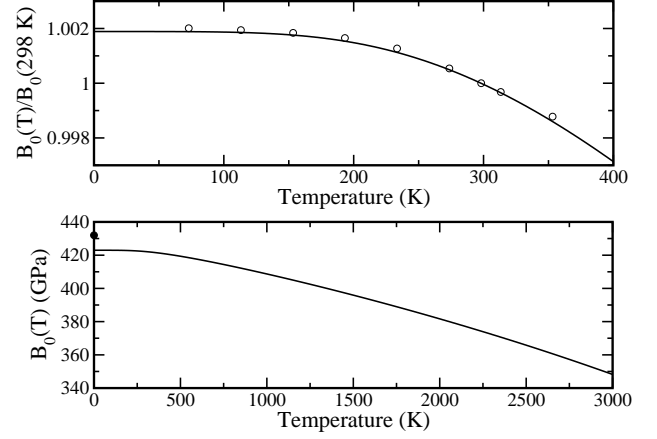


FIG. 22: Lower panel: Bulk modulus $B_0(T)$ of diamond as a function of temperature. The filled circle indicates the value of the bulk modulus (as in Table I) before accounting for zero-point motion. Upper panel: theoretical (solid line) and experimental values (Ref. 72, open circles) for the ratio between $B_0(T)$ and $B_0(298\text{K})$ in the low temperature regime.

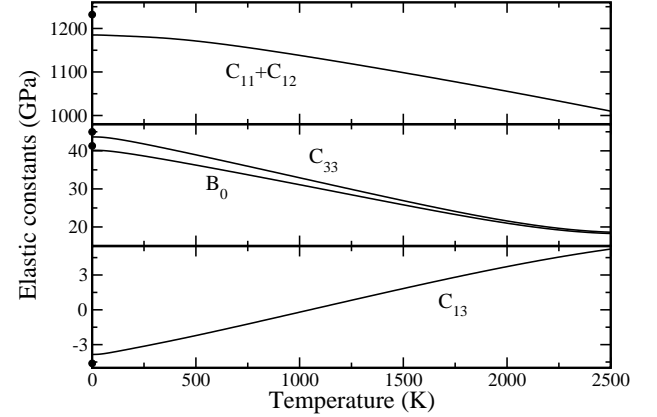


FIG. 23: Elastic constants of graphite ($C_{11} + C_{12}$, C_{13} , C_{33}) and bulk modulus (B_0) as a function of temperature. The filled circles (at 0 K) indicate their ground state values (as in Table II) before accounting for zero-point motion.

V. CONCLUSION

We have presented a full ab-initio study of the structural, vibrational and thermodynamic properties of diamond, graphite and graphene, at the DFT-GGA level and using the quasiharmonic approximation to derive thermodynamic quantities. All our results are in very good agreement with experimental data: the phonon dispersions are well-reproduced, as well as most of the elastic constants. In graphite, the C_{33} elastic constant and the α phonon dispersions (calculated here with GGA for the first time) were found to be in good agreement with experimental results provided the calculations were performed at the experimental α . Only the C_{13} constant remains in poor agreement with experimental data.

The decay of the long-ranged interatomic force con-

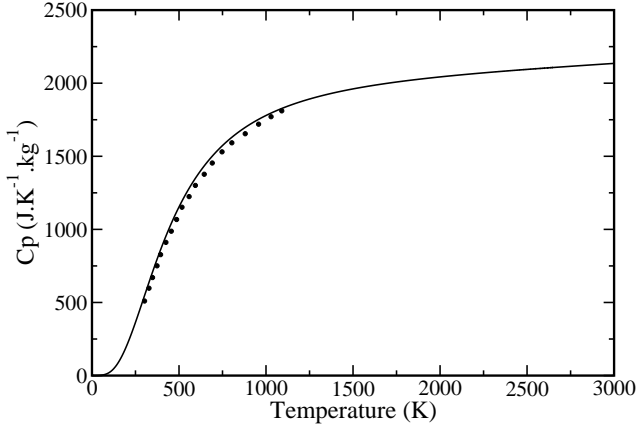


FIG. 24: Constant pressure heat capacity for diamond (solid line). Experimental results are from Refs. 49 and 73 (circles), as reported by Ref. 65.

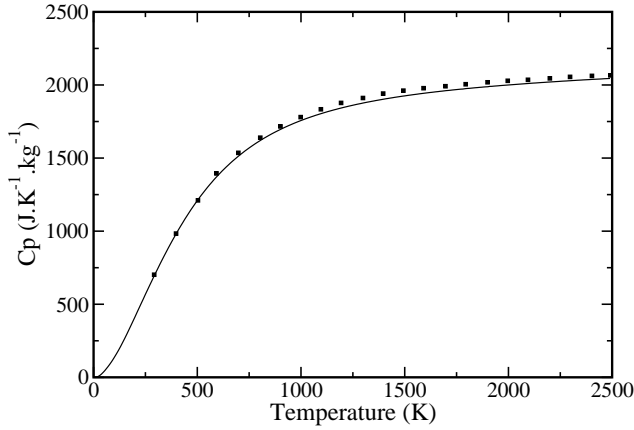


FIG. 25: Constant pressure heat capacity for graphite (solid line). Experimental results are from Ref. 74 (squares), as reported by Ref. 75.

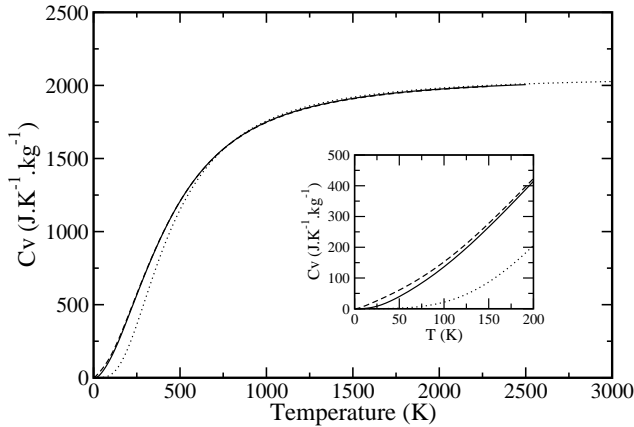


FIG. 26: Constant volume heat capacity for graphite (solid line), graphene (dashed line) and diamond (dotted line). The inset shows an enlargement of the low temperature region.

stants was analyzed in detail. It was shown that interactions in the (110) direction in diamond are longer-ranged than these in other directions, as is characteristic of the zincblende and diamond structures. For graphene and graphite, in-plane interactions are even longer-ranged and phonon frequencies sensitive to the truncation of the interatomic force constants.

Thermodynamical properties such as the thermal expansion, temperature dependence of elastic moduli and specific heat were calculated in the quasi-harmonic approximation. These quantities were all found to be in close agreement with experiments, except for the out-of-plane thermal expansion of graphite at temperatures higher than 150 K. Graphite shows a distinctive in-plane negative thermal expansion coefficient that reaches the minimum around room temperature, in very good agreement with experiments. This effect is found to be three times as large in graphene. In both cases, the mode Grüneisen parameters show that the ZA "bending" acoustic modes are responsible for the contraction, in a direct manifestation of the membrane effect predicted by Lifshitz⁶¹ in 1952. These distinctive features will likely affect the thermodynamical properties of single-walled and multiwall carbon nanotubes^{41,66,67}.

Acknowledgments

The authors gratefully acknowledge support from NSF-NIRT DMR-0304019 and the Interconnect Focus Center MARCO-DARPA 2003-IT-674. Nicolas Mounet personally thanks the Ecole Polytechnique of Palaiseau (France) and the Fondation de l'Ecole Polytechnique for their help and support.

- ⁶³ T. Aizawa, R. Souda, S. Otani, Y. Ishizawa, and C. Oshim a, Phys. Rev. B 42, 11469 (1990).
- ⁶⁴ W. Kohn, Phys. Rev. Lett. 2, 393 (1959).
- ⁶⁵ C. P. Herrero and R. Ramirez, Phys. Rev. B 63, 024103 (2000).
- ⁶⁶ N. Mounet and N. Marzari, in preparation.
- ⁶⁷ Y. K. Kwon, S. Berber, and D. Tom anek, Phys. Rev. Lett. 92, 015901 (2004).
- ⁶⁸ G. L. Belenkii, R. A. Suleim anov, N. A. Abdullaev, and V. Y. Stenshaiber, Sov. Phys. Solid State 26, 2142 (1984).
- ⁶⁹ N. A. Abdullaev, Phys. Solid State 43, 727 (2001).
- ⁷⁰ N. A. Abdullaev, R. A. Suleim anov, M. A. Aldzhanov, and L. N. A lieva, Phys. Solid State 44, 1859 (2002).
- ⁷¹ K. Karch, T. Dietrich, W. Windl, P. Pavone, A. P. Mayer, and D. Strauch, Phys. Rev. B 53, 7259 (1996).
- ⁷² H. J. M cSkin in and P. A ndreatch, J. Appl. Phys. 43, 2944 (1972).
- ⁷³ A. C. Victor, J. Chem. Phys. 36, 1903 (1962).
- ⁷⁴ R. R. Hultgren, Selected Values of the Therm odynam ic Properties of the Elements (American Society for Metals, Metals Park, Ohio, 1973).
- ⁷⁵ L. E. Fried and W. M. Howard, Phys. Rev. B 61, 8734 (2000).